

# RMPE: Regional Multi-person Pose Estimation

Haoshu Fang, Shuqin Xie, Cewu Lu\*  
Shanghai Jiao Tong University

## Abstract

Multi-person pose estimation in images taken in the wild is a challenging problem, where human detector inevitably suffers from errors both in localization and recognition. These undesirable errors would ultimately result in failures of most CNN-based single-person pose estimators. In this paper, a novel regional multi-person pose estimation (RMPE) framework is proposed to facilitate single-person pose estimator in presence of the inaccurate human detector. In particular, our framework consists of three novel techniques, namely, symmetric spatial transformer network (SSTN), deep proposals generator (DPG) and parametric pose non-maximum suppression (NMS). Extensive experimental results have demonstrated the validity and effectiveness of the proposed approach. In comparison to the state-of-the-art approach, the proposed approach significantly achieves **16% increase in mAP on MPII (multi person) dataset [2]**. Our model and source codes are **publicly available**.<sup>†</sup>

## 1. Introduction

In practice, recognizing multi-person human pose in wild image is a challenging task, which is much more difficult than single person pose estimation (SPPE) [27, 28, 19, 21, 34]. The major difficulty is to locate and recognize poses simultaneously, where persons in a group could occlude each other.

In recent literature [6, 24, 16], this problem is approached by developing part-based method, which could achieve state-of-the-art detection performance. All the body parts (e.g. hand, leg and head) are firstly detected in an independent manner and then assembled into poses by making use of image-conditioned pairwise terms. Although those methods could partly address body part occlusion problem, they inevitably lost the capability of recognizing parts from a global pose view due to the mere utilization of second-order parts dependence.

Inspired by this problem, we aim to globally estimate all

parts by investigating holistic person region. This higher-level semantic understanding can also help to identify occlusion. Fortunately, existing object detectors [12, 11, 26] can roughly localize single person regions. We are then able to infer human parts globally. In fact, some earlier works [25, 13] are based on a two-stage framework, which carry out detection of single person regions and detection of single person pose sequentially. However, this straightforward pipeline fails to obtain desirable performance, even if the state-of-the-art object detector (e.g. Faster RCNN [26]) and SPPE (e.g. stacked hourglass model [21]) are employed. This is mostly due to the issue that SPPE network is rather vulnerable to human detection error, including those visually acceptable errors. For example, in task of object detection, the boxes having 0.5 overlap with ground truth can be declared as correct detection. However, directly applying SPPE on them would result in failure of pose estimation, where an example is shown in Figure 1. Moreover, redundant human detection would directly generate redundant pose candidates as shown in Figure 2. As a result, these redundant candidates may overlap with other persons in multi-person scenarios, making non-maximum suppression less effective

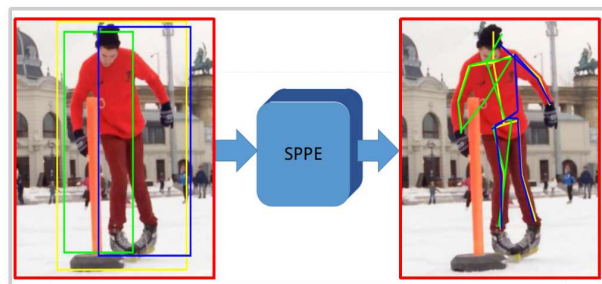


Figure 2. Redundant human detections. The left figure is detection results of object detector, the right image is the pose estimations corresponding to detected boxes. It shows the results of multiple pose proposals in one single person.

To address these problems, a regional multi-person pose estimation approach is proposed in this paper. The objective is to facilitate the SPPE to perform well in presence of imperfect human detector. Firstly, symmetric STN structure is designed to extract high-quality single person regions,

\*Cewu Lu is the corresponding author: lu-cw@cs.sjtu.edu.cn

<sup>†</sup><https://github.com/Fang-Haoshu/rmpe>

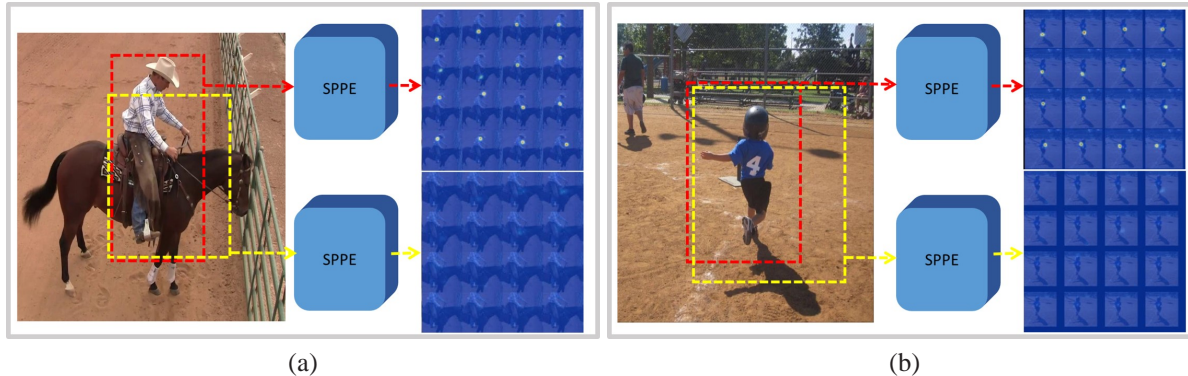


Figure 1. Localization Error. The dashed red box is the ground truth box, the yellow box is a proposal with  $IoU > 0.5$  over the red box. The heatmaps are outputs of SPPE [21] corresponding to these two boxes. It can be observed that the SPPE could not generate correct results on the yellow box proposal.

which are fed to the SPPE subsequently. In this network, a novel spatial re-mapping highway is introduced for optimization. Secondly, a parametric pose NMS is proposed. As a matter of fact, pose NMS is much more challenging than bounding box NMS, since pose matching metric should be well defined and parameters should be carefully chosen. Our parametric pose NMS could desirably extract the pose matching metric into 4 key parameters and fit the model in a data-driven manner. Finally, training samples are augmented by using a novel deep proposals generator. By leveraging a dizygotic-Siamese network, it can simulate large amounts of human proposals produced by human detectors.

It should be noted that our framework is applicable to different human detectors and single person pose estimators. Experimental results have demonstrated that our method could outperform the state-of-the-art method by 16% in mAP on standard MPII dataset (multi-person) [2]. Ablation studies have been conducted to further validate the effectiveness of proposed techniques. We will make our source models and codes publicly available to support reproducible research.

## 2. Related Work

We will briefly review single person pose estimation. Subsequently, two basic multi-person pose estimation frameworks will be discussed.

### 2.1. Single Person Pose Estimation

For single human pose estimation, the input should be a single person dominated image and output would be body parts. Various classic approaches have focused on pictorial structure models. For example, simple tree models[27, 36, 32] have been demonstrated to be extremely efficient for solving this task. Due to the independency assumption of the output variable, they generally fail to capture additional dependencies between body parts. To ad-

dress this problem, multiple tree models[33] and random forest models [28, 7] have been proposed. More recently, deep learning becomes a promising technique for computer vision, where human pose estimation is of no exception. This technique is introduced to the area of human pose estimation by DeepPose (Toshev *et al*)[30] for the first time. After that, various DNN based models[22, 10] and CNN based models[18, 29, 21, 3, 34] have been proposed, which could perform rather well on related benchmarks. Apart from simply solving the human pose estimation problem, researchers also proposed unified frameworks for simultaneous human parsing and pose estimation[8, 23]. For single person pose estimation, these methods could only perform well in the cases where the person has been correctly located. However, this assumption cannot be satisfied in practice.

### 2.2. Multi Person Pose Estimation

**Part-based Framework** Previous works are mainly based on part-based framework[6, 13, 31, 24, 16]. In [6], Chen *et al.* presented an approach to parse largely occluded people by graphical model, which models humans as flexible compositions of body parts. In [13], Gkiox *et al* used k-poselets to jointly detect people and predict locations of the poses. The final pose localization can be predicted by a weighted average of all activated pose-lets. Pishchulin *et al.* [24] proposed a DeepCut framework to first detect all body parts, and then label and assemble these parts to be a person via integral linear programming. In [16], a stronger part detector based on ResNet[14] and a better incremental optimization strategy is used to further improve the performance, where the method also achieves large speedup. However, this method still costs 485 seconds to test an image on MPII multi-person full set, which has made it impractical for real world applications. In summary, part-based frameworks perform well in some scenarios; however, it cannot perform in a global manner for pose estimation. This observation has inspired us to make im-

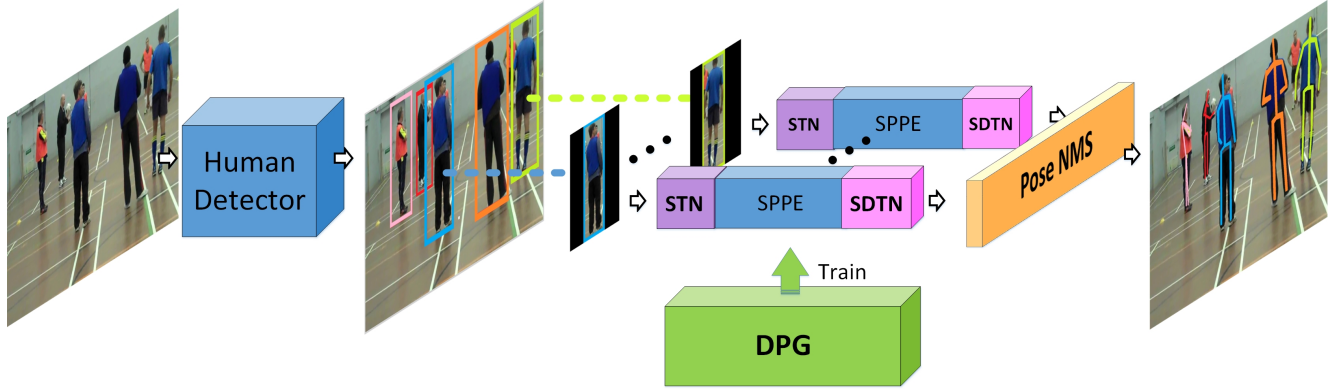


Figure 3. Pipeline of our proposed approach. A **Symmetric STN** consists of **STN** and **SDTN**. They are configured before and after the **SPPE**. Detected human proposal is received by **STN** and **SDTN** outputs pose proposal. Finally, a **parametric Pose NMS (p-Pose NMS)** is carried out before final predictions. Different from traditional training method, we train the **SSTN+SPPE** module with images generated by **deep proposals generator (DPG)**. Note that we still draw multiple **SPPEs** just for better understanding.

provements.

**Two-step Framework** Our work is similar to the previous works [25, 13] in the way that it firstly detects different people in the image and independently predicts pose. In our work, we use the powerful CNN based single person to predict poses, while Pishchulin *et al.* [25] used conventional pictorial structure models to perform pose estimation. In [16], a similar two-stage pipeline is proposed that uses Faster R-CNN as their human detector and a unary DeepCut for pose estimations. However, the method in [16] can only achieve 51.0 in mAP on MPII dataset, which is significantly lower than our results (69.2 mAP). With the development of object detection and single person pose estimation, this two-step framework is still a good candidate for pose estimation. However, maximizing the power of SPPE with human detection error is still an open problem.

In conclusion, the two-step framework demonstrates its potential for multi-person pose estimation task. However, single person detection network should be facilitated in presence of imperfect human regions.

### 3. Our Approach

Our objective is to estimate multi-person poses in a wild image, where human location is unknown in the testing phase. In many cases, persons always occlude with each other. Firstly, we briefly present a straight-forward two-step framework, where basic human detector and single person pose estimator are introduced. Subsequently, our proposed regional multi-person pose estimation (RMPE) is presented. In the following sections, “single person image” refers to the image contains a dominant person. The training and testing on single person images are carried out by SPPE.

#### 3.1. Straight-forward Two-step Framework

In the straight-forward framework, human proposal is firstly detected by human detector and single person pose estimator is subsequently applied to those human proposals individually. The framework is sketched in Figure. 4.

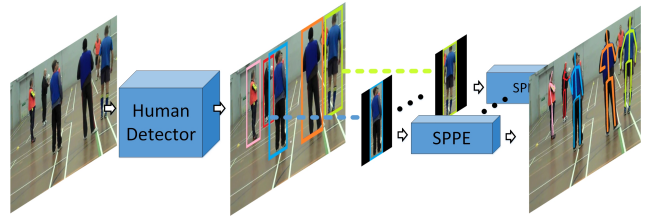


Figure 4. Straight-forward two-step framework. After the bounding boxes of detected persons are given, we apply SPPE on them individually. Note that the SPPE for detected persons remains to be the same. Here, we draw multiple SPPEs for better understanding.

In this paper, the SSD [20] is employed as our human detector, since it effectively and efficiently performs object detection. We use the stacked hourglass model [21] as the single person pose estimator due to its superior performance.

**Discussion** Although the object detection has achieved substantial progress in recent years, most of human proposals obtained by the existing detector are still not qualified enough to be the input of SPPE. In presence of imperfect human detectors, SPPE should be robust and be able to perform well. In this way, our system can be flexible to different human detectors and SPPEs. As improvement of those two components, the overall multi-person pose estimation will be improved as a final result. Towards this end, our regional multi-person pose estimation is proposed, where the details are presented in following sections.

### 3.2. Regional Multi-person Pose Estimation

The pipeline of proposed RMPE is sketched in Figure 3. The human proposals obtained by human detector are fed into “Symmetric STN + SPPE” module and pose proposals will be generated individually. These proposals will be further refined by **parametric Pose NMS**. To augment the existing training samples, **deep proposals generator** is designed to largely augment training samples. Based on this big picture, we will present our three main technical contributions as follows.

#### 3.2.1 Symmetric STN

As mentioned, human proposals provided by human detector are not well-suited to SPPE. This is because SPPE is specifically trained on single person image set. In this section, a novel Symmetric STN is introduced, where the power of SPPE can be fully leveraged. It attempts to feed SPPE with single person image extracted from imperfect human proposals.

**Proposal Extension** In order to guarantee the entire person region to be extracted, human proposal is extended with 20% along both height and width direction. In this way, it can be found that the most of single persons can be fully contained in our extended proposals. For brevity, “human proposal” refers to “extended human proposal” in the following.

**STN and SDTN** A spatial transformer network [17](STN) is used help SPPE to extract high quality single person images. STN has been demonstrated to be excellent at automatically selecting interesting region to improve final performance. More specifically, the STN performs a 2D affine transformation and the point-wise transformation can be mathematically expressed as

$$\begin{pmatrix} x_i^s \\ y_i^s \end{pmatrix} = [\theta_1 \quad \theta_2 \quad \theta_3] \begin{pmatrix} x_i^t \\ y_i^t \\ 1 \end{pmatrix} \quad (1)$$

where  $\theta_1$ ,  $\theta_2$  and  $\theta_3$  are vector in  $\mathbb{R}^2$ .  $\{x_i^s, y_i^s\}$  and  $\{x_i^t, y_i^t\}$  are coordinates before and after transformation, respectively. After SPPE, the resulting pose is mapped into original human proposal image. Naturally, a spatial de-transformer network (SDTN) is required to be employed. SDTN simply computes the  $\gamma$  for de-transform and generates grids based on  $\gamma$ .

$$\begin{pmatrix} x_i^t \\ y_i^t \end{pmatrix} = [\gamma_1 \quad \gamma_2 \quad \gamma_3] \begin{pmatrix} x_i^s \\ y_i^s \\ 1 \end{pmatrix} \quad (2)$$

Since SDTN is the inverse procedure of STN, we can obtain

$$[\gamma_1 \quad \gamma_2] [\theta_1 \quad \theta_2] = \begin{bmatrix} 1 & 0 \\ 0 & 1 \end{bmatrix} \quad (3)$$

$$[\gamma_1 \quad \gamma_2] \theta_3 + \gamma_3 = \begin{bmatrix} 0 \\ 0 \end{bmatrix} \quad (4)$$

By extracting single person image as input, we can maintain the power of off-the-shelf SPPE which is well trained on single person images. The module of “Symmetric STN”+“SPPE” is shown in Figure 5.

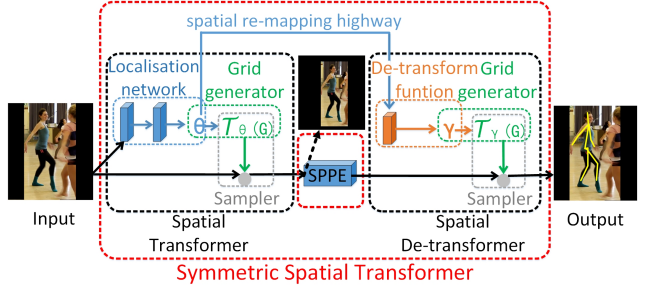


Figure 5. A detailed illustration of Symmetric STN architecture. The structure enclosed by the red dotted line is SSTN, consists of STN and SDTN. STN is described in paper [17]. For SDTN, it takes  $\theta$  generated by localization net and compute the  $\gamma$  for de-transform. The blue arrow from STN to SDTN is spatial re-mapping highway. For more details of grid generator and sampler please refer to the original paper [17].

**Spatial Re-mapping Highway** For optimization purpose, we attempt to allow information flow between STN and SDTN. Specifically, we jointly optimize STN and SDTN by back propagation technique. A spatial re-mapping highway is constructed to connect STN and SDTN. Solving Eqn. (3)(4) can be easily done and parameter  $\gamma$  can be obtained.

$$[\gamma_1 \quad \gamma_2] = [\theta_1 \quad \theta_2]^{-1} \quad (5)$$

$$\gamma_3 = -1 \times [\gamma_1 \quad \gamma_2] \theta_3 \quad (6)$$

For back propagation of SDTN  $\frac{\partial J(W,b)}{\partial \theta}$  can be derived by

$$\begin{aligned} \frac{\partial J(W,b)}{\partial [\theta_1 \quad \theta_2]} &= \frac{\partial J(W,b)}{\partial [\gamma_1 \quad \gamma_2]} \times \frac{\partial [\gamma_1 \quad \gamma_2]}{\partial [\theta_1 \quad \theta_2]} \\ &+ \frac{\partial J(W,b)}{\partial \gamma_3} \times \frac{\partial \gamma_3}{\partial [\gamma_1 \quad \gamma_2]} \times \frac{\partial [\gamma_1 \quad \gamma_2]}{\partial [\theta_1 \quad \theta_2]} \end{aligned} \quad (7)$$

$$\frac{\partial J(W,b)}{\partial \theta_3} = \frac{\partial J(W,b)}{\partial \gamma_3} \times \frac{\partial \gamma_3}{\partial \theta_3} \quad (8)$$

and  $\frac{\partial [\gamma_1 \quad \gamma_2]}{\partial [\theta_1 \quad \theta_2]}$ ,  $\frac{\partial \gamma_3}{\partial \theta_3}$  can be easily derived from Eqn. (5)(6).

**Discussion** The spatial re-mapping highway from SDTN to STN can largely shorten the information propagation distance from loss-end to STN. With this shortcut, easier parameter adjustment for STN can be facilitated to reduce

the final loss. In this manner, SDTN is not only a simple re-mapping process of STN, but can also jointly optimize with STN and SPPE. In our experiment, we adopt SqueezeNet[15] as our localization network, since it is small yet powerful enough to extract desired features.

**Parallel SPPE** To further enforce STN extract single person image, we add a parallel SPPE in training phrase. For the parallel SPPE, we specify its labels to be pose on single person image. It shares the same STN with Symmetric STN. In this way, we can push STN to focus on correct area and extract high quality single person image. The training pipeline is illustrated in Figure 6. We minimize the sum error of parallel SPPE and symmetric STN together. In testing phase, we discard parallel SPPE and forward in Symmetric STN only. In experiment section, we verify that this additional scheme improve the system indeed.

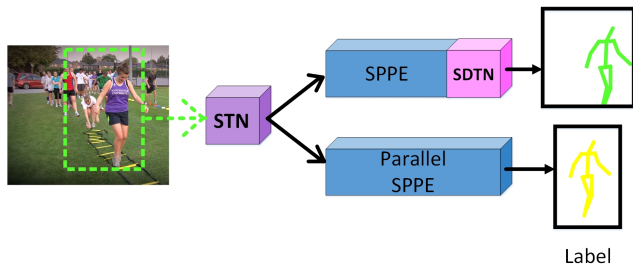


Figure 6. Our training strategy with parallel SPPE. The green dashed box is human proposal. A centered located pose label is specified to the parallel SPPE, which could further encourage STN to extract single person image.

### 3.2.2 Deep Proposals Generator

**Data Augmentation** SSTN+SPPE module (symmetric STN + SPPE) should be trained on human proposals generated by human detector. Otherwise, the module may not work properly in testing phase for human detector. However, the number of human proposals is small in training dataset, since human detector can only produce about 20 ~ 30 proposals per image. This quantity is not sufficient for training a good model. Therefore, proper augmentation of the training data should be considered, where the augmented data should follow same distribution as human detector’s output.

**Insight** A novel deep proposals generator is proposed to produce a large amount of high quality augmented samples. We seek a network whose input is a pose and box proposal to directly predict the possibility that input box proposal is generated by human detector with respect to input pose. We randomly sample a huge number of region proposals. The

network will select part of them as augmented samples according to their output scores (possibilities). In this way, a large number of high quality training samples can be obtained. In particular, box proposal is represented by the proposal indicator image that assigns pixels inside proposal as black and outside ones as white. Pose is captured by labeling different joints with different colors.

**Architecture** The network architecture we adopted is a dizygotic-Siamese network (see Figure 7), whose network structure is similar to Siamese network [4]. Similar to Siamese network, the feature vector of both inputs can be obtained,  $\ell_1$  norm pairwise distance between them can be computed, and a Gaussian function could directly measure the matching error. The only difference is that dizygotic-Siamese network does not share weights of two sub-networks, since two input images are substantially different. Our dizygotic-Siamese is trained on the ground truth pairs (pose image and their corresponding human proposals generated by human detector). The details of training are presented in section 4.1.1.

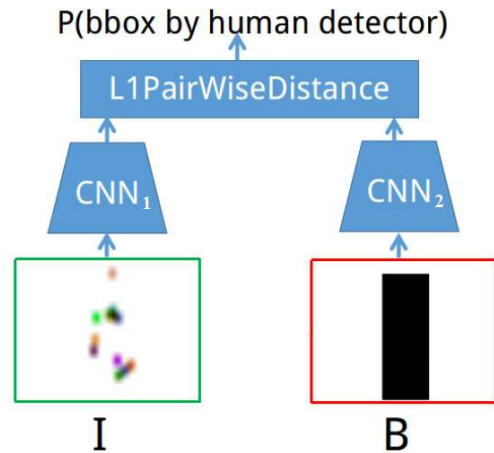


Figure 7. The architecture of Deep Proposals Generator. Taking a pose image(I) and a proposal indicator(B) as input, it outputs the probability that the proposal is generated from human detector. Human joints are labeled with different colors. The labeling processes are described in experiment detail.

### 3.2.3 Parametric Pose NMS

Human detector inevitably generates redundant detections, which will results in redundant poses. Therefore, pose non-maximum suppression (NMS) is generally required to eliminate those redundant detections. As before, the pose  $P_i$  with  $m$  joints is denoted as  $\{\langle k_i^1, c_i^1 \rangle, \dots, \langle k_i^m, c_i^m \rangle\}$ , where  $k_i^j$  and  $c_i^j$  are the  $j^{th}$  location and confidence score of joints.

**NMS scheme** We revisit pose NMS as follows. Firstly, most confident pose is selected as reference, and some poses close to it are eliminated by an appropriate *elimination criterion*. This process is re-carried out in the remaining poses set until all poses are eliminated (or selected). Finally, we report all selected reference poses.

**Elimination Criterion** As can be seen, the most important thing for the elimination criterion is to determine a pose should be eliminated or not (close to reference pose or not). This problem can be transformed to define a good pose distance metric  $d(P_i, P_j|\Lambda)$  and a threshold  $\eta$ , where  $\Lambda$  are parameter set of function  $d(\cdot)$ . Our elimination criterion can be written as,

$$f(P_i, P_j|\Lambda, \eta) = \mathbb{1}[d(P_i, P_j|\Lambda, \lambda) \leq \eta] \quad (9)$$

If  $d(\cdot)$  is smaller than  $\eta$ , the output of  $f(\cdot)$  should be 1, which indicates that pose  $P_i$  should be eliminated with respect to reference pose  $P_j$ .

**Pose Distance** Now, we present the distance function  $d_{pose}(P_i, P_j)$ . As earlier, we define the soft matching function as

$$K_{Sim}(P_i, P_j|\sigma_1) = \begin{cases} \sum_n \tanh \frac{c_i^n}{\sigma_1} \cdot \tanh \frac{c_j^n}{\sigma_1}, & \text{if } k_j^n \text{ is within } \mathcal{B}(k_i^n) \\ 0 & \text{otherwise} \end{cases} \quad (10)$$

where  $\mathcal{B}(k_i^n)$  is box center at  $k_i^n$  and the size of box follows the standard PCK metric[35], namely, 0.1 of human size. The tanh operation will filter out a large amount of low-confidence scores. If two joints are both confident, the output will be close 1. This distance softly counts the number of joints matching between poses.

The spatial distance among parts are also considered, which can be written as

$$H_{Sim}(P_i, P_j|\sigma_2) = \sum_n \exp\left[-\frac{(k_i^n - k_j^n)^2}{\sigma_2}\right] \quad (11)$$

By combining Eqn (10) and (11), the final distance function can be written as,

$$d(P_i, P_j|\Lambda) = K_{Sim}(P_i, P_j|\sigma_1) + \lambda H_{Sim}(P_i, P_j|\sigma_2) \quad (12)$$

where  $\lambda$  is weight balancing two distances and  $\Lambda = \{\sigma_1, \sigma_2, \lambda\}$ . Note that previous pose NMS [6] set pose distance parameters and threshold manually. In contrast, our parameters can be determined in a data-driven manner.

**Optimization** Given the detected redundant poses, the four parameters in eliminate criterion  $f(P_i, P_j|\Lambda, \eta)$  are

optimized to achieve optimum mAP in training set. Since exhaustive search in the 4D space is intractable, we optimize two parameters by fixing other two parameters in an iterative manner. Once convergence, the elimination criterion will be determined. It will be applied in the testing phase.

### 3.3. Testing

In testing stage, the human proposal is detected by SSD [20] object detector. Subsequently, the human proposals are fed as the input of SSTN+SPPE module individually and pose proposals are generated as outputs. Those redundant pose proposals are eliminated by parametric pose NMS for final pose detection. Parallel SPPE will be discarded in testing phase.

## 4. Experiments

The proposed method is qualitatively and quantitatively evaluated on three standard multi-person datasets with large occlusion cases, i.e., MPII [2] and WAF [9] as suggested in [16], and MSCOCO 2016 keypoints challenge dataset[1]. Our algorithms are implemented using Caffe and Torch7 on a server with 4 TITAN X GPUs. All the models and source codes will be published.

**MPII (multi-person).** We evaluated our method on the challenging benchmark MPII Human Pose(multi-person), which consists of 3844 training and 1758 testing groups with both occluded and overlapped people. Moreover, it contains more than 28K training samples for single person pose estimation. All the training data in the single person dataset are used to fine-tune the SPPE.

**WAF** This dataset is a multi-person pose dataset which consists of 350 training and 175 testing images with occluded and overlapped people. The upper-body of every approximately upright and frontal person is annotated.

**MSCOCO Keypoints Challenge** This challenge requires localization of person keypoints in challenging, uncontrolled conditions. It consists of 100k training and 80k testing human instances. The training set consists of over 1 million total labeled keypoints.

### 4.1. Results

#### 4.1.1 MPII Experimental Details.

We describe how the DPG network is trained. We randomly sample 30 patches around each ground truth pose. These patches that have IoU with ground truth human bounding boxes larger than 0.5 are labeled as negative samples. In

	Head	Shoulder	Elbow	Wrist	Hip	Knee	Ankle	Total	time [s/frame]
Iqbal&Gall [31]	58.4	53.9	44.5	35.0	42.2	36.7	31.1	43.1	10
DeeperCut [16]	78.4	72.5	60.2	51.0	57.2	52.0	45.4	59.5	485
ours, 2-stack SPPE	85.5	81.5	71.3	62.1	65.0	62.7	56.5	69.2	<b>0.8</b>
<b>ours, 8-stack SPPE</b>	<b>87.7</b>	<b>85.1</b>	<b>77.3</b>	<b>68.5</b>	<b>73.5</b>	<b>70.9</b>	<b>63.8</b>	<b>75.3</b>	<b>0.8</b>

Table 1. Results on MPII multi-person full test set (mAP). Note that the 2-stack SPPE and 8-stack SPPE have the same depth but different structure. For more details please refer to [21]

	Head	Shoulder	Elbow	Wrist	Hip	Knee	Ankle	Total	time [s/frame]
DeepCut[24]	73.1	71.7	58.0	39.9	56.1	43.5	31.9	53.5	57995
Iqbal&Gall[31]	70.0	65.2	56.4	46.1	52.7	47.9	44.5	54.7	10
DeeperCut [16]	87.9	84.0	71.9	63.9	68.8	63.8	58.1	71.2	230
ours, 2-stack SPPE	89.7	85.8	75.3	68.8	67.7	69.8	59.2	73.8	0.75
<b>ours, 8-stack SPPE</b>	<b>89.4</b>	<b>88.5</b>	<b>81.0</b>	<b>75.4</b>	<b>73.7</b>	<b>75.4</b>	<b>66.5</b>	<b>78.6</b>	<b>0.75</b>

Table 2. Results on MPII multi-person 288 sub test set (mAP)

	Head	Shoulder	Elbow	Wrist	Total
Chen&Yuille [6]	83.3	56.1	46.3	35.5	55.3
DeepCut [24]	76.6	80.8	73.7	73.6	76.2
DeeperCut [16]	92.6	81.1	75.7	78.8	82.0
<b>ours, 2-stack SPPE</b>	<b>95.6</b>	<b>83.5</b>	<b>88.3</b>	<b>81.6</b>	<b>87.3</b>

Table 3. Results on WAF Multi-Person set (AP)

Team	AP	$AP^{50}$	$AP^{75}$	$AP^M$	$AP^L$
CMU-Pose[5]	<b>61.8</b>	<b>84.9</b>	<b>67.5</b>	57.1	<b>68.2</b>
G-RMI	60.5	82.2	66.2	57.6	66.6
DL-61	54.4	75.3	50.9	<b>58.3</b>	54.3
R4D	51.4	75	55.9	47.4	56.7
umich_v1	46	74.6	48.4	38.8	55.6
Caltech	40.2	65.2	41.9	34.9	49.2
ours, 8-stack SPPE	57.2	81.0	64	53.6	63.3

Table 4. Results on MSCOCO Keypoint challenge (AP)

contrast, the human proposals by human detector are all labeled as positive samples. It should be noted that a much larger number of negative samples are obtained compared to the number of positive sample. This would induce significant imbalance between positive and negative samples. In our case, the ratio between negative samples and positive samples is around 24:1. To approximately balance the positive and negative samples, we divide the negative samples into 24 parts. Thus, hard negative mining training is used as follows [12]. Only the patches labeled as positive are used as augmented training samples.

#### 4.1.2 Comparison with State-of-the-Art

**Results on MPII dataset.** We evaluate our method on full MPII Multi-Person test set. Compared to the previous state-of-the-art results, our method could achieve significant improvements over the previous method by **16 mAP**. Quantitative results are given in Table 1. The improvement gained by replacing the 2-stack SPPE to 8-stack SPPE demonstrates that our framework are applicable to different SPPE. Notably, we achieve an average accuracy of 70 mAP on identifying difficult joints such as wrists, elbows, ankles, and knees, which is 18 mAP higher than the most recent state-of-the-art result. More specifically, we reach a final accuracy of 70.9 mAP for the knee and an accuracy of 63.8 mAP for the ankle. We present some of our results in Figure 8. These results demonstrate that our method can accurately predict pose in multi-person images. More results are presented in supplementary materials.

In terms of computational speed, our method is also much faster than the part-based method that can achieve the state-of-the-art performance[16]. The whole procedure is speed up 600 times. For our two-stage framework, the forward time for each frame depends on the number of humans. On MPII Multi-human full data set, the average number of humans per image is 3.6 and thus our average forward time is 0.8 seconds.

For comparison, we also evaluate our method on the subset of 288 testing images as in[24], the results are given in Table 2.

**Results on WAF dataset.** We evaluate our method on WAF test set by using our model trained on MPII datasets. There are two reasons that re-training of our model is not carried out on WAF training set. First, the WAF datasets is

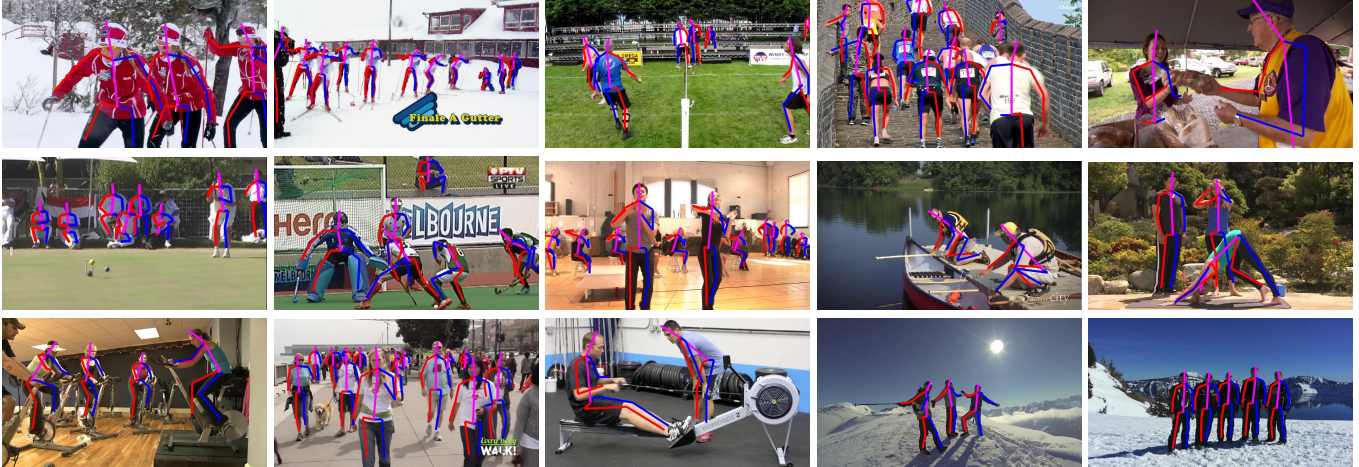


Figure 8. Some results of our model’s predictions.

not big enough for training our SPPE model (350 training samples only). Second, a bounding box cropping the whole person is required to train the SPPE model, which cannot be extracted from the data of WAF since it only offers labeling of upper body. Note that we adopt the more realistic AP evaluation measure, suggested by [16]. Compared to other approaches [6, 24, 16], our method achieves significant improvements and outperforms previous method by 5.3 mAP. Quantitative results are given in Table 3.

**Results on MSCOCO Keypoints dataset.** We finetune the SPPE on MSCOCO Keypoints training + validating set. Quantitative results on test-dev set are given in Table 4. Our method yields a considerable result. Note that with similar human detector and SPPE, our method outperforms R4D and Caltech with a great margin, which proves the effectiveness of our proposed framework.

#### 4.2. Ablation studies

We evaluate the effectiveness of the three proposed techniques, i.e., symmetric STN, deep proposals generator (DPG) and parametric Pose NMS. The ablative studies have been conducted by removing them from pipeline or replacing them with conventional solvers on MPII Multi-human dataset. Of course, the straightforward two-step method without those three techniques is also compared for fairness. We conduct our experiment using the 2-stack SPPE, which is more memory efficient than the 8-stack one.

**Symmetric STN** To understand the importance of symmetric STN, we demonstrate that the transformed image is more suitable for the SPPE network. Two experiments are conducted to validate this argument. In the first experiment, we remove the SSTN including parallel SPPE from

the pipeline in both training and testing phases. In the second experiment, we only remove the parallel SPPE and keep the symmetric STN structure. Both of the results are shown in Table 5. We observe apparent performance degradation without parallel SPPE, which implies that parallel SPPE with single person image labels would strongly encourage the STN to extract single person regions with minimized errors.

**Deep Proposals Generator** We demonstrate that our deep proposals generator also plays an important role for our system. In this experiment, we remove the data augmentation by DPG from in our training phase. The result is shown in Table 5. We can see that the final mAP drops to 62.6%. This is because that, although SSTN can transform the image to make it more suitable for SPPE, it is required that SSTN+SPPE module should be adaptive to human detector. DPG can allow the model to fit human proposal that can be used in testing phase. Without DPG, the whole SSTN module has much less data to learn during training phase, where the degraded performance occurs.

**Parametric Pose NMS** Our previous experiment evaluates the performance of the parametric Pose NMS. Since pose NMS is an independent module, we can directly remove it from our final model. The experimental results are shown in Table 5. As we can see, the mAP drops significantly if the parametric Pose NMS is removed. The reason is that the increase in the number of redundant poses will ultimately decrease our precision. We note that the previous pose NMS can also eliminate redundant detection to some extent. The state-of-the-art pose NMS algorithm [6] is used to replace our parametric Pose NMS, where the result is given in Table 5. This scheme performs less effective compared to ours, since the parameter learning is missing.

	Head	Shoulder	Elbow	Wrist	Hip	Knee	Ankle	Total
<b>RMPE, 2-stack SPPE</b>	<b>85.5</b>	<b>81.5</b>	<b>71.3</b>	<b>62.1</b>	<b>65.0</b>	<b>62.7</b>	<b>56.5</b>	<b>69.2</b>
rm SSTN+parallel SPPE	81.5	78.8	67.3	58.9	61.6	58.1	49.7	65.1
rm parallel SPPE only	82.1	79.8	69.0	59.3	61.0	59.6	52.8	66.2
rm DPG	81.8	77.8	66.9	57.4	60.4	53.9	40.1	62.6
rm PoseNMS	76.7	73.9	64.5	56.5	59.7	58.2	52.7	63.2
PoseNMS [6]	82.1	78.8	69.1	60.3	63.1	61.1	55.1	67.1
straight forward two-steps	71.4	68.3	58.8	51.4	49.9	52.3	50.2	57.5

Table 5. Results of our ablation experiments on MPII multi-person test set. “rm X” means removing X module from our pipeline. “PoseNMS [6]” reports the result that use the pose NMS algorithm in [6]

## 5. Conclusion

In this paper, a regional multi-person pose estimation method is proposed, which can significantly outperform the state-of-the-art method for multi-person human pose estimation in terms of accuracy and efficiency. It validates the potential of the two-step framework, i.e., human detector + SPPE, if SPPE can be adapted to human detector. Towards this end, our RMPE framework consists of three novel techniques: symmetric STN, deep proposals generator and parametric pose NMS. In particular, deep proposals generator is used to largely argument the training data by leveraging the power of deep neural network. The SPPE become robust to human localization errors due to the utilization of symmetric STN. Finally, parametric pose NMS could desirably reduce redundant detections. In our future work, it would be interesting to explore the possibility of using our framework to improve human detector in turn.

## References

- [1] Mscoco keypoint challenge 2016. <http://mscoco.org/dataset/keypoints-challenge2016>. 6
- [2] M. Andriluka, L. Pishchulin, P. Gehler, and B. Schiele. 2d human pose estimation: New benchmark and state of the art analysis. In *CVPR*, 2014. 1, 2, 6
- [3] V. Belagiannis and A. Zisserman. Recurrent human pose estimation. *arXiv preprint arXiv:1605.02914*, 2016. 2
- [4] J. Bromley, J. W. Bentz, L. Bottou, I. Guyon, Y. LeCun, C. Moore, E. Säckinger, and R. Shah. Signature verification using a siamese time delay neural network. *International Journal of Pattern Recognition and Artificial Intelligence*, 7(04):669–688, 1993. 5
- [5] Z. Cao, T. Simon, S.-E. Wei, and Y. Sheikh. Realtime multi-person 2d pose estimation using part affinity fields. *arXiv preprint arXiv:1611.08050*, 2016. 7
- [6] X. Chen and A. L. Yuille. Parsing occluded people by flexible compositions. In *Proceedings of the IEEE Conference on Computer Vision and Pattern Recognition*, pages 3945–3954, 2015. 1, 2, 6, 7, 8, 9
- [7] M. Dantone, J. Gall, C. Leistner, and L. Van Gool. Human pose estimation using body parts dependent joint regressors. In *CVPR*, pages 3041–3048, 2013. 2
- [8] J. Dong, Q. Chen, X. Shen, J. Yang, and S. Yan. Towards unified human parsing and pose estimation. In *CVPR*, pages 843–850, 2014. 2
- [9] M. Eichner and V. Ferrari. We are family: Joint pose estimation of multiple persons. In *European Conference on Computer Vision*, pages 228–242. Springer, 2010. 6
- [10] X. Fan, K. Zheng, Y. Lin, and S. Wang. Combining local appearance and holistic view: Dual-source deep neural networks for human pose estimation. In *CVPR*, pages 1347–1355. IEEE, 2015. 2
- [11] R. Girshick. Fast r-cnn. In *Proceedings of the IEEE International Conference on Computer Vision*, pages 1440–1448, 2015. 1
- [12] R. Girshick, J. Donahue, T. Darrell, and J. Malik. Rich feature hierarchies for accurate object detection and semantic segmentation. In *Computer Vision and Pattern Recognition*, 2014. 1, 7
- [13] G. Gkioxari, B. Hariharan, R. Girshick, and J. Malik. Using k-poselets for detecting people and localizing their keypoints. In *Proceedings of the IEEE Conference on Computer Vision and Pattern Recognition*, pages 3582–3589, 2014. 1, 2, 3
- [14] K. He, X. Zhang, S. Ren, and J. Sun. Deep residual learning for image recognition. *CVPR*, 2016. 2
- [15] F. N. Iandola, M. W. Moskewicz, K. Ashraf, S. Han, W. J. Dally, and K. Keutzer. Squeezenet: Alexnet-level accuracy with 50x fewer parameters and 1mb model size. *arXiv preprint arXiv:1602.07360*, 2016. 5
- [16] E. Insafutdinov, L. Pishchulin, B. Andres, M. Andriluka, and B. Schiele. DeeperCut: A Deeper, Stronger, and Faster Multi-Person Pose Estimation Model. In *European Conference on Computer Vision (ECCV)*, May 2016. 1, 2, 3, 6, 7, 8
- [17] M. Jaderberg, K. Simonyan, A. Zisserman, et al. Spatial transformer networks. In *Advances in Neural Information Processing Systems*, pages 2017–2025, 2015. 4
- [18] A. Jain, J. Tompson, M. Andriluka, G. W. Taylor, and C. Bregler. Learning human pose estimation features with convolutional networks. *arXiv preprint arXiv:1312.7302*, 2013. 2
- [19] L. Ladicky, P. H. Torr, and A. Zisserman. Human pose estimation using a joint pixel-wise and part-wise formulation. In *CVPR*, pages 3578–3585, 2013. 1
- [20] W. Liu, D. Anguelov, D. Erhan, C. Szegedy, and S. Reed. SSD: Single Shot MultiBox Detector. In *ECCV*, 2016. 3, 6

- [21] A. Newell, K. Yang, and J. Deng. Stacked hourglass networks for human pose estimation. *arXiv preprint arXiv:1603.06937*, 2016. [1](#), [2](#), [3](#), [7](#)
- [22] W. Ouyang, X. Chu, and X. Wang. Multi-source deep learning for human pose estimation. In *CVPR*, June 2014. [2](#)
- [23] S. Park and S.-C. Zhu. Attributed grammars for joint estimation of human attributes, part and pose. In *ICCV*, pages 2372–2380, 2015. [2](#)
- [24] L. Pishchulin, E. Insafutdinov, S. Tang, B. Andres, M. Andriluka, P. Gehler, and B. Schiele. Deepcut: Joint subset partition and labeling for multi person pose estimation. In *IEEE Conference on Computer Vision and Pattern Recognition (CVPR)*, June 2016. [1](#), [2](#), [7](#), [8](#)
- [25] L. Pishchulin, A. Jain, M. Andriluka, T. Thormählen, and B. Schiele. Articulated people detection and pose estimation: Reshaping the future. In *Computer Vision and Pattern Recognition (CVPR), 2012 IEEE Conference on*, pages 3178–3185. IEEE, 2012. [1](#), [3](#)
- [26] S. Ren, K. He, R. Girshick, and J. Sun. Faster R-CNN: Towards real-time object detection with region proposal networks. In *Advances in neural information processing systems*, pages 91–99, 2015. [1](#)
- [27] B. Sapp, A. Toshev, and B. Taskar. Cascaded models for articulated pose estimation. In *ECCV*, pages 406–420. Springer, 2010. [1](#), [2](#)
- [28] M. Sun, P. Kohli, and J. Shotton. Conditional regression forests for human pose estimation. In *CVPR*, pages 3394–3401. IEEE, 2012. [1](#), [2](#)
- [29] J. J. Tompson, A. Jain, Y. LeCun, and C. Bregler. Joint training of a convolutional network and a graphical model for human pose estimation. In *NIPS*, pages 1799–1807, 2014. [2](#)
- [30] A. Toshev and C. Szegedy. Deeppose: Human pose estimation via deep neural networks. In *CVPR*, 2014. [2](#)
- [31] J. G. Umar Iqbal. Multi-person pose estimation with local joint-to-person associations. In *European Conference on Computer Vision Workshops 2016 (ECCVW'16) - Workshop on Crowd Understanding (CUW'16)*, 2016. [2](#), [7](#)
- [32] F. Wang and Y. Li. Beyond physical connections: Tree models in human pose estimation. In *CVPR*, pages 596–603, 2013. [2](#)
- [33] Y. Wang and G. Mori. Multiple tree models for occlusion and spatial constraints in human pose estimation. In *ECCV*, pages 710–724. Springer, 2008. [2](#)
- [34] S.-E. Wei, V. Ramakrishna, T. Kanade, and Y. Sheikh. Convolutional pose machines. In *Proceedings of the IEEE Conference on Computer Vision and Pattern Recognition*, pages 4724–4732, 2016. [1](#), [2](#)
- [35] Y. Yang and D. Ramanan. Articulated human detection with flexible mixtures of parts. *IEEE Transactions on Pattern Analysis and Machine Intelligence*, 35(12):2878–2890, 2013. [6](#)
- [36] X. Zhang, C. Li, X. Tong, W. Hu, S. Maybank, and Y. Zhang. Efficient human pose estimation via parsing a tree structure based human model. In *ICCV*, pages 1349–1356. IEEE, 2009. [2](#)